26

Algebraic Reconstruction and Post-processing in Incomplete Data Computed Tomography: From X-rays to Laser Beams

Alexander B. Konovalov, Dmitry V. Mogilenskikh, Vitaly V. Vlasov and Andrey N. Kiselev
Russian Federal Nuclear Centre – Zababakhin Institute of Applied Physics Russia

1. Introduction

Methods of computed tomography are well developed and widely used in medicine and industry. If tomographic data are complete, it is possible to reconstruct the images with sub-millimeter resolution. If the data are incomplete, tomograms may blur, i.e. their resolution degrades, noise increases and artifacts form. The situation is worst if measurement data are so poor that the system of equations which describe the discrete reconstruction problem appears to be strongly underdetermined. In this situation, images of acceptable quality can be obtained with algorithms that regularize the solution and use a priori information about the object, and do post-processing of reconstructed tomograms also with the use of a priori information, as a rule. This chapter provides two examples demonstrating the reconstruction of the internal structure of an object from strongly incomplete measurement data: few-view computed tomography (FVCT) and diffuse optical tomography (DOT) of strongly scattering media. The problem of reconstruction from a small number of views (<10) arises, for example, in experimental plasma research (Pickalov & Melnikova, 1995) or nondestructive testing (Subbarao et al., 1997). DOT is now deemed to hold much promise for cancer detection (Arridge, 1999; Hawrysz & Sevick-Muraca, 2000; Yodh & Chance, 1995). Here the strong incompleteness of data is caused by the fact that the number of source-receiver relations that define the number of measurements is strictly limited. Despite that these types of tomography use different wavelength bands (X-ray and near infrared) and different mathematical models (linear and non-linear), we think it is not only possible, but also interesting to consider them together because in both cases we successfully use similar reconstruction algorithms and similar post-processing methods. The unique possibility to do that comes from the fact that in case of DOT, we use a simplified reconstruction method (Konovalov et al., 2003; 2006b; 2007; Lyubimov et al., 2002; 2003) reducing the inverse problem to a solution of the integral equation with integration along a conditional photon average trajectory (PAT) – an analog of the Radon transform in projection tomography.

In case of FVCT, we use actual data from measurements in a simple experimental radiography setup (Konovalov et al., 2006a). The FVCT procedure is simulated by rotation of the object from exposure to exposure about the centre of the reconstruction region. For

Source: Vision Systems: Applications, ISBN 978-3-902613-01-1
Edited by: Goro Obinata and Ashish Dutta, pp. 608, I-Tech, Vienna, Austria, June 2007

objects, we use a spatial resolution test and an iron sphere with quasi-symmetric cracks resulted from shock compression.
In case of DOT, we use model data from the numerical solution of a time-dependent diffusion equation with an instantaneous point source (time-domain measurement technique). We consider a traditional geometry where sources and receivers are on the boundary of a scattering object in the form of a flat layer (Konovalov et al., 2006b). The object contains periodic structures created by circular absorbing inhomogeneities.
In both cases, the inverse problem is solved using algebraic reconstruction techniques (additive and multiplicative) which we modernized to attain the better convergence of the iterative reconstruction process (Konovalov et al., 2006a; 2006b). Procedures used to calculate the weight matrices are described in detail. Solution correction formulas are modified with respect to distributions of weight sums and solution correction numbers over image elements. Weighted smoothing is performed at each iteration of solution approximation. We use a priori information on whether the solution is non-negative and on the presence of structure-free zones in the reconstruction region.
For post-processing of reconstructed tomograms, we use space-varying restoration (Konovalov et al., 2007), methods for enhancing informativity of images based on its nonlinear color interpretation (Mogilenskikh, 2000) and methods for estimating image informativity based on binary operations and visualization algorithms (Mogilenskikh & Pavlov, 2002; Mogilenskikh, 2003).
Results of investigation help decide how spatial resolution depends on the degree of data incompleteness and draw inferences on whether the modified reconstruction techniques are effective and on the investigated post-processing methods are capable of making tomograms more informative.
The chapter is organized as follows. Section 2 gives a general formulation of the tomography problem. It is shown that the inverse problem of DOT, like the problem of reconstruction from X-ray projections, can be reduced to a solution of an integral equation with integration along the trajectory. The Section describes a discrete model of a 2D reconstruction problem and modernized algebraic techniques. Section 3 gives examples of 2D reconstruction from experimental radiographic data and model diffusion projections from optical inhomegeneities. The Section makes a quantitative analysis of the spatial resolution of tomograms reconstructed from strongly incomplete data. Section 4 describes post-processing methods and gives examples of their use. Section 5 draws inferences and outlines further research in the area.

2. Generality of our approach to reconstruction from strongly incomplete data

2.1 From the Radon transform to the fundamental equation of the PAT method

The problem of reconstruction in computed tomography is known to be formulated as follows: find the best estimation of a function of spatial coordinates $f(\mathbf{r})$, called an object function, from a discrete set of its measured projections. Generally, each projection can be written as a weighting integral

$$g = \int_{\infty} w(\mathbf{r}) f(\mathbf{r}) d^3 r , \tag{1}$$

where $w(\mathbf{r})$ is a weighting function which depends on source and receiver positions in space, the type of actual physical measurements and the way of data recording.
In transmission X-ray tomography where the spatial distribution of the extinction coefficient $\mu(\mathbf{r})$ is reconstructed, it is usually assumed that the weighting function is unity along a line L connecting a point source and a point receiver, and zero elsewhere. Then expression (1) turns into the linear integral

$$g = \int_L \mu(\mathbf{r})\, dl\,. \tag{2}$$

In computed tomography, it is known as the Radon transform. Integral (2) is inverted with a linear reconstruction model implemented with the use of both integral algorithms (Kak & Slanay, 1988) and algebraic techniques (Herman, 1980).
Divergence of the probing beam in, for example, proton (Hanson, 1981; 1982) or diffraction (Devaney, 1983) tomography makes it necessary to consider not a line but a narrow 3D strip of a finite length. In this case, it may be needed to change from linear integration (2) to volume one (1) and pose restrictions on the use of the linear reconstruction model.
Diffuse optical tomography (DOT) of strongly scattering media is the most demonstrative example of non-linear tomography. Laser beams used for probing undergo multiple scattering, so photon trajectories are not regular and photons are distributed in the entire volume V under study. As a result, each point in the volume significantly contributes to the detected signal. If, for example, we deal with absorbing inhomogeneities of tissues examined by pulsed probing with the time-domain measurement technique, integral (1), in the approximation of the perturbation theory by Born or Rytov, takes the form (Lyubimov et al., 2002; 2003)

$$g(t) = \int_V \left\{ \int_0^t vP[\mathbf{r},\tau \,|\, (\mathbf{r}_s,0) \to (\mathbf{r}_d,t)]\, d\tau \right\} \delta\mu_a(\mathbf{r})\, d^3 r\,, \tag{3}$$

where t is the time-gating delay of the receiver recording the signal, v is the light velocity in the media, $P[\mathbf{r},\tau \,|\, (\mathbf{r}_s,0) \to (\mathbf{r}_d,t)]$ is the density of the conditional probability that a photon migrating from a space-time source point $(\mathbf{r}_s,0)$ to a space-time receiver point $(\mathbf{r}_d,t)$ reaches an intermediate space point $\mathbf{r}$ at time τ, and $\delta\mu_a(\mathbf{r})$ is the distribution function of the absorbing inhomogeneities. Local linearization of the inverse problem of DOT is usually done with multi-step reconstruction algorithms based on the variational formulation of the radiation transport equation (or its diffusion approximation). The Newton-Raphson algorithm with the Levenberg-Marquardt iterative procedure (Arridge, 1999) is a typical example of these algorithms. The multi-step algorithms provide a relatively high spatial resolution (~5 mm) for diffusion tomograms, but they are not as fast as required for real-time diagnostics because we have to solve a forward problem, i.e. the problem of propagation of radiation through matter, many times by adjusting at each linearization step the matrix of coefficients of a system of algebraic equations describing the discrete reconstruction model.
There is a unique opportunity to accelerate the reconstruction procedure: to change in expression (3) from volume integration to integration along a conventional line connecting point source and point receiver. Using a probabilistic interpretation of light transfer by

means of the conditional probability density P, Lyubimov et al. (2002; 2003) proved that integral (3) could be presented as

$$g(t) = \int_L \frac{\langle \delta\mu_a(\mathbf{r}) \rangle_P}{v(l)} dl \,, \tag{4}$$

where L is a curve defined by coordinates of the mass centers of the instantaneous distributions P in accordance with

$$\mathbf{R}(\tau) = \int_V \mathbf{r} P[\mathbf{r}, \tau \,|\, (\mathbf{r}_s, 0) \to (\mathbf{r}_d, t)] d^3 r \,, \tag{5}$$

which we call a photon average trajectory (PAT). Here l is a distance along the PAT, $v(l)$ is the relative velocity of the mass center of the distribution P along the PAT as a function of l, $\langle \cdot \rangle_P$ is the operator of averaging over the spatial distribution P. Integral equation (4) is a fundamental equation of the photon average trajectories method (PAT method) in case of time-domain measurement technique. It is an analog of Radon transform (2) and can be inverted with the fast algorithms of projection tomography. In other words, converting (3) into (4) offers an opportunity to change from multi-step to one-step reconstruction in the sense that the system of algebraic equations describing the discrete reconstruction model is only inverted once and hence, to achieve significant savings in computational time.
Equation (4) has definitely a number of differences from equation (2), specifically:
(a) Integration is performed along not a straight but curved line;
(b) Under integral (4), there is a weighting distribution $1/v(l)$ which depends on spatial coordinates; and
(c) Trajectory integration is applied not to the object function itself, but to a function averaged over the spatial distribution P.
The latter means that the reconstructed image is degraded by a priori blur which requires additional work, i.e. post-processing of tomogram. With the above differences, it becomes clear that the inversion of equation (4) with the linear reconstruction model requires certain assumptions which may affect the quality of reconstructed images. Nevertheless, our earlier studies (Konovalov et al., 2003; 2006b; 2007; Lyubimov et al., 2002; 2003) and results presented in Sections 3 and 4 show that the PAT method is quite effective in the context of the tomogram quality versus reconstruction speed trade-off.

2.2 Discrete image reconstruction model

In medical applications of X-ray computed tomography, equation (2) is usually inverted by means of integral reconstruction algorithms such as the backprojection algorithm with convolution filtering (Kak & Slanay, 1988). In FVCT where the number of views is small, reconstruction with the integral algorithms gives aliasing artifacts which are present on tomograms as "rays" tangential to reproduced structures (Palamodov, 1990). Different smoothing and regularization methods can be applied to remove these artifacts which strongly restrict the resolution of small details. But the quality of reconstructed images still remains far from satisfactory.
It is also difficult to invert equation (4) with integral algorithms. Here problems arise from not only incomplete data, but also from curved PATs. Our attempts to implement the

backprojection algorithm for diffusion tomograms (Konovalov et al., 2003; 2007; Lyubimov et al., 2003) are based on the assumption that the PATs are almost straight lines inside the scattering object. But with this approach it is impossible to reconstruct the spatial distribution of absorbing inhomogeneities near boundaries where photons escape from the object like an avalanche and the PATs strongly bend.

In this case, both in FVCT and in DOT, it is appropriate to use iterative algebraic algorithms implementing a discrete reconstruction model. In this chapter, without loss of generality, we will only consider examples of 2D reconstruction, i.e. reconstructions of 2D images. The generalized discrete model of 2D reconstruction is formulated traditionally (Herman, 1980). Let us establish a Cartesian grid for square image elements so that it covers the object. Assume that the reconstructed object function takes a constant value f_{kl} in an element with indices k and l (hereafter, (k,l)-cell). Let L_{ij} be a straight line or PAT connecting i-source and j-receiver, and g_{ij} be a projection measured by j-receiver from i-source. Then the discrete reconstruction model can be characterized by a system of linear algebraic equations

$$g_{ij} = \sum_{k,l} W_{ijkl} f_{kl}, , \tag{6}$$

where W_{ijkl} is the weight contributed by the (k,l)-cell to the measured value g_{ij}. In the traditional setup of 2D reconstruction, the weight W_{ijkl} is proportional to the length of intersection of the trajectory L_{ij} with the (k,l)-cell (Herman, 1980; Lyubimov et al., 2002).

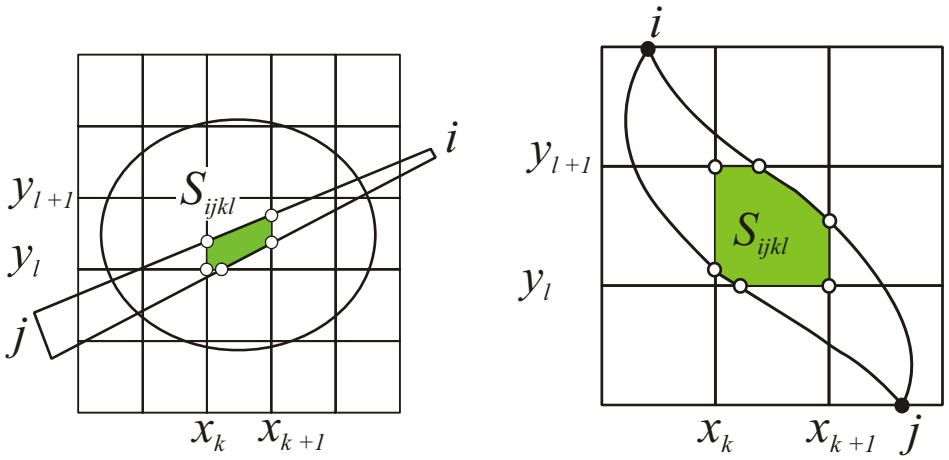

Figure 1. Calculation of weights: (a) X-ray tomography; (b) DOT

In this case, the matrix of coefficients of system (6) (hereafter, weight matrix) appears to be highly sparce because each trajectory intersects very few cells. This fact markedly worsens

convergence of algorithms used to solve system (6) that is strongly underdetermined due to incomplete data. To reduce the number of zero elements in the matrix, we modernized the method for calculation of W_{ijkl} having changed the infinite narrow trajectory by a strip of a finite width (Konovalov et al., 2006a; 2006b).

In X-ray tomography, the strip is a long trapeze (Figure 1(a)). Its bases are source aperture (the linear size of the focal spot) and receiver aperture (as a rule, the intrinsic resolution of the recording system). In this case, the weights can be calculated with the formula

$$W_{ijkl} = S_{ijkl} / \delta , \tag{7}$$

where S_{ijkl} is the area of intersection of the strip corresponding to i -source and j -receiver (hereafter, (i, j) -strip) with the (k,l) -cell, and δ is the linear size of the cell. It is obvious that the calculation of S_{ijkl} for trapezoidal strips must not cause difficulty.

The situation is more complicated in DOT. The configuration and size of the appropriate strip must be selected with account for the spatial distribution of the trajectories of photons migrating from the point $(\mathbf{r}_s,0)$ to the point $(\mathbf{r}_d,t)$. According to the above statistical model, the most probable trajectories are distributed in a zone defined by the standard root-mean-square deviation (RMSD) from the PAT in accordance with the formula

$$\Delta(\tau) = \left\{ \int_V \left|\mathbf{r} - \mathbf{R}(\tau)\right|^2 P[\mathbf{r}, \tau \,|\, (\mathbf{r}_s,0) \to (\mathbf{r}_d,t)]\, d^3 r \right\}^{1/2} . \tag{8}$$

This zone is shaped as a banana (Lyubimov et al., 2002; Volkonskii, 1999) with vertices at the points of source and receiver localizations on the boundary of the scattering object. Therefore, for the (i, j) -strip we take a banana-shaped strip (Figure 1(b)) whose width is directly proportional to the RMSD: $\varepsilon(\tau) = \gamma \cdot \Delta(\tau)$. The problem is thus reduced to finding statistical characteristics (5) and (8) of photon trajectories. Note that the exact analytical calculation of $\mathbf{R}(\tau)$ and $\Delta(\tau)$ is difficult for even simple configurations such as a circle or a flat layer. The use of numerical techniques is undesirable because of the necessity to save computational time. Therefore, a number of simplifying assumptions should be done.

Lyubimov et al. (2002) and Volkonskii et al. (1999) propose to approximate the PAT by a three-segment broken line whose end segments are orthogonal to the boundary of the scattering object and the middle segment connects the end ones. This approach is effective if inhomogeneities are located inside the object, but causes distortions if inhomogeneities are near the boundaries where the PATs bend. In this chapter we configure banana-shaped strips in the geometry of a flat layer using a simplified analytical approach based on the analysis of PAT bending near a plane boundary. The approach uses the time-dependent radiation transport equation in the diffusion approximation. Konovalov et al. (2006b) showed that in the case where a instantaneous point source was in a homogeneous half-space (a half-plane in 2D) $y \geq 0$ at a point $(0, y_0)$ and a receiver was at a point $(x_0,0)$ on the boundary $y = 0$, coordinates of the mass center of the distribution P, moving from the source point to the receiver point could be expressed as

$$\begin{cases} X(\tau) = x_0 \tau / t \\ Y(\tau) = y_0 \left\{ \left[1 + \dfrac{\tau}{t}\left(\dfrac{\alpha}{2} - 1 \right) \right] \mathrm{erf}\left(\dfrac{t-\tau}{\alpha\tau} \right)^{1/2} + \left[\dfrac{\alpha\tau(t-\tau)}{\pi t^2} \right]^{1/2} \exp\left(-\dfrac{t-\tau}{\alpha\tau} \right) \right\}, \end{cases} \quad (9)$$

where $\alpha = 4Kvt/y_0^2$, K is the diffusion coefficient of the media, $\mathrm{erf}(\xi)$ is the probability integral. If assume that PAT bending near the plane (straight line) of a source S is similar to bending near the plane (straight line) of a receiver D and there is no influence of the opposite boundary, analytical expressions (9) can be easily used to construct the PAT for the flat layer geometry (Figure 2). Indeed, the mass center passes the distance SO and the distance OD during the time $t/2$. If the mass center moved in the half-space $y \geq 0$ from a point S_0 to the point D through the point O, the time $t/2$ would correspond to the distance S_0O. Since component velocity along the X-axis is constant, the point S_0 lies on the perpendicular SS' to the media boundaries. The distance S_0S' can be found through the numerical solution of the equation $Y|_{\tau=t/2} = d/2$, where d is the width of the layer, for y_0 (see expressions (9)). After that the distance OD is calculated with (9) and the distance SO is obtained through its symmetric reflection about the point O.

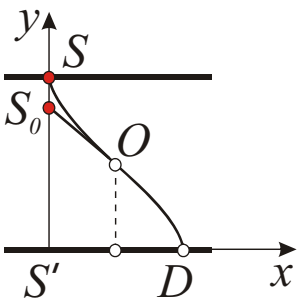

Figure 2. PAT construction for a flat layer

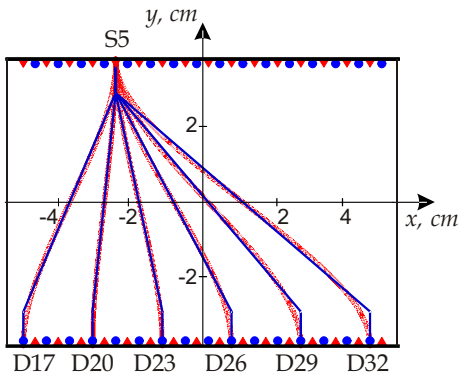

Figure 3. Geometry of data recording for a rectangular object

Figure 3 shows the geometry of data recording we chosen for simulations. Red triangles denote the positions of sources and blue circles do the positions of receivers. It also shows, as examples, six average trajectories reproduced with the above algorithm for $t = 3000$ ps and optical parameters $K = 0.066$ cm and $v = 0.0214$ cm/ps. Blue lines show piecewise-linear approximations of the PATs. Coordinates of the indicated sources and receivers (in centimeters) are as follows: S5 – (-2.52, 4), D17 – (-5, -4), D20 – (-3.06, -4), D23 – (-1.13, -4), D26 – (0.81, -4), D29 – (2.74, -4), D32 – (4.68, -4). In this chapter we study the probing regime in transmission, i.e. only relations between sources and receivers located on the opposite boundaries of the object are considered. The total number of average trajectories therefore

equals to 32×16 (32 sources and 16 receivers). In the reconstruction we will vary the number of sources to study how the spatial resolution depends on the degree of data incompleteness.

High accuracy of RMSD calculation is not crucial for the construction of banana-shaped strips. Therefore, in accordance with the inference of Volkonskii et al. (1999) that RMSD is actually independent of the form of the object, we can use the following simple formula for infinite space:

$$\Delta(\tau) \cong \left[2Kv(t-\tau)\tau / t \right]^{1/2}. \tag{10}$$

Boundaries of banana-shaped strips are defined as follows.

(a) Define a set of discrete times $\{\tau_p\}$.

(b) Construct perpendiculars to tangential lines at PAT points corresponding to times $\{\tau_p\}$ (Figure 4).

(c) Lay off sections of the length $\varepsilon(\tau_p)$ in both directions along each perpendicular.

(d) Construct lines connecting the points which we obtained for different $\{\tau_p\}$.

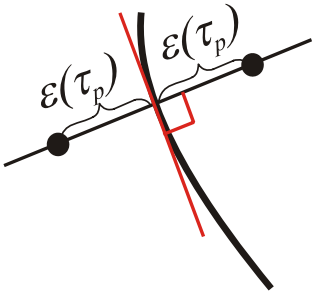

Figure 4. Definition of boundaries for banana-shaped strip

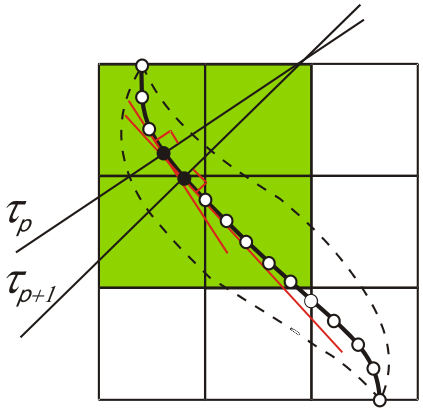

Figure 5. Definition of the discrete relative velocities of mass center of the distribution P

Boundaries of the strips are thus defined by piecewise-linear functions. To calculate the areas S_{ijkl}, we find the points where the strip boundaries intersect the sides of the cell. A polygon with vertices at the obtained points and cell nodes is treated as the intersection of the (i,j)-strip and the (k,l)-cell (Figure 1(b)). Weights are calculated with the formula

$$W_{ijkl} = S_{ijkl} / (v_{ijkl}\,\delta) \tag{11}$$

where v_{ijkl} is the discrete velocity of the mass center of the distribution P for the (i,j)-strip and the (k,l)-cell. Analytically, the velocities $v(\tau_p)$ are determined through

differentiation of expressions (9). The array of discrete values $\{v_{ijkl}\}$ is defined with the following algorithm.

(a) Define a set of discrete times $\{\tau_p\}$.

(b) Construct perpendiculars to tangential lines at points of L_{ij} corresponding to the times $\{\tau_p\}$ (Figure 5).

(c) Assign a loop for p, in which the following sequence of steps is performed:

- Find cells where the (i, j)-strip intercepts a strip created by two neighbor perpendiculars corresponding to the times τ_p and τ_{p+1}. In Figure 5, these cells are shown in green.
- To all cells found, assign a value which equals the velocity averaged over two times: $[v(\tau_p) + v(\tau_{p+1})]/2$.
- If some value v_{ijkl}^{old} has already been assigned to a cell, it is updated with the formula

$$v_{ijkl} = \frac{v_{ijkl}^{old} \cdot N + v_{ijkl}^{new}}{N+1}, \tag{12}$$

where v_{ijkl}^{new} is the new value and N is the number of previous updates.

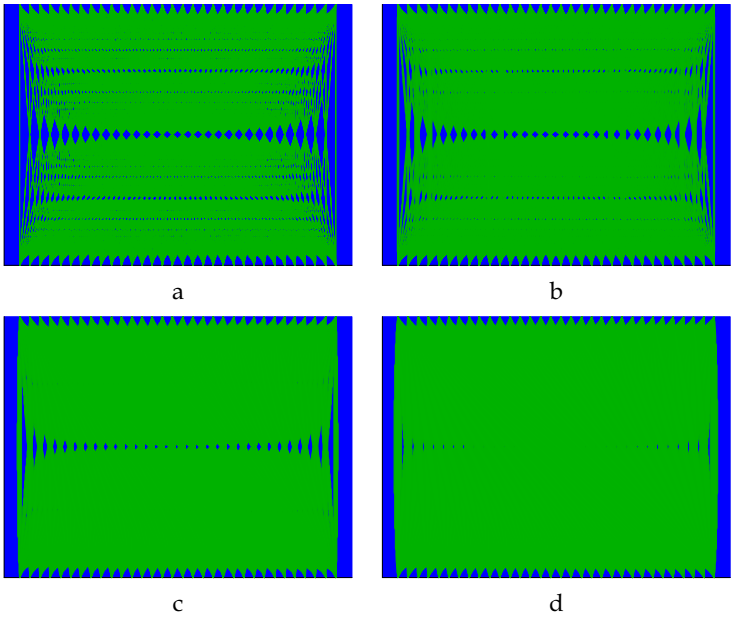

Figure 6. The area of the object filled with banana-shaped strips for different values of coefficient γ: (a) – 0; (b) – 0.05; (c) – 0.15; and (d) – 0.25

(d) All PATs are searched sequentially and, for each of them, the procedure is repeated beginning from step (b).

The proportionality coefficient $\gamma \in (0, 1)$ which defines the width of the banana-shaped strip is selected from a condition dictating that all strips must sufficiently fill the area of the object. Figure 6 shows the filling of the rectangular object presented in Figure 3 for ratio of sources and receivers (hereafter, measurement ratio) 32×16 and γ equal to 0, 0.05, 0.15, and 0.25. In Figure 6(a), (b), and (c), there are extended regions with no strips (shown in blue). This means that, if the grid is of high resolution, there are cells where corrections won't be introduced during the process of reconstruction. In Figure 6(d) these regions are very small in size which minimizes the probability that "dead" cells will appear. That is why we reconstruct the absorbing inhomogeneities embedded in the scattering object shown in Figure 3 using banana-shaped strips whose width is $\varepsilon(\tau) = 0.25\Delta(\tau)$.

It should be noted that the problem of area filling in FVCT is not as decisive as in DOT if even the strips are very narrow. Despite the small number of views, the number of strips corresponding to one view is rather large (> 100).

2.3 Algebraic reconstruction techniques and methods of their modification

When selecting an algorithm to invert system (6), we must remember that in case of very incomplete data, the system appears to be strongly underdetermined. That is why the problem of solution regularization is of great importance in the context of the need to approximate the solution correctly and hence, to obtain tomograms which are free of artifacts. It is well known that the minimum of artifacts corresponds to the minimum of information contained in images. Under these circumstances, it seems appropriate to do reconstruction with an approach based on entropy optimization (Levine & Tribus, 1978). In this chapter we study the multiplicative algebraic reconstruction technique (MART) which implements the entropy maximum method. The problem of solution regularization is formulated as follows. Find the array of values $\{f_{kl}\}$ which satisfies system (6) and the conditions

$$f_{kl} \geq 0, \quad \left(\sum_{k,l} f_{kl} \ln f_{kl} \right) \to \max . \tag{13}$$

For the purpose of comparison and to demonstrate advantages of the MART, we also consider a well-known additive algebraic reconstruction technique (AART) which does not optimize entropy.

Both MART and AART are based on an iterative procedure of correction of certain initial approximation $\{f_{kl}^{(0)}\}$. At each $(s+1)$-iteration trajectories (strips) from one source only are considered. Thus, the correction is introduced into the elements of the approximation $\{f_{kl}^{(s)}\}$ which correspond to the cells intersected by the given strips. Upon a transition from one iteration to another, the sources are searched cyclically. Original formulas for the correction of the s-th approximation to the solution are written as follows (Herman, 1980)

$$\begin{aligned}
&\text{MART}: \quad f_{kl}^{(s+1)} = f_{kl}^{(s)} \cdot \left(g_{ij} \Big/ \sum_{k,l} W_{ijkl} f_{kl}^{(s)} \right)^{\lambda W_{ijkl} / \delta} \\
&\text{AART}: \quad f_{kl}^{(s+1)} = f_{kl}^{(s)} + \lambda \frac{g_{ij} - \sum_{k,l} W_{ijkl} f_{kl}^{(s)}}{\|\mathbf{W}\|_F^2} W_{ijkl} \,,
\end{aligned} \tag{14}$$

where $\lambda \in (0,1)$ is the parmeter which controls the rate of iterative process convergence and $\|\cdot\|_F$ is the Frobenius norm.

Our experience of using the algebraic techniques in FVCT (Konovalov et al., 2006a) and DOT (Konovalov et al., 2006b; Lyubimov et al., 2002) suggests that a number of modifications to formulas (14) are needed to improve convergence in case of strongly incomplete data. So, expressions (14) does not allow for

(a) the non-uniform distributions of weight sums and solution correction numbers over the cells; and

(b) any a priori information on the spatial distribution of reproduced structures.

As a result, both algorithms including the MART with regularization (13) often converge to a wrong solution. Because of the incorrect redistribution of intensity, images exhibit distinct artifacts which are often present in the regions where the structures are actually absent.

To avoid these shortcomings, we here use the following formulas for modified algebraic techniques

Step 1

$$\begin{aligned}
&\text{MART}: \quad f_{kl}^{(s+1)} = w_{kl} \cdot f_{kl}^{(s)} \cdot \left(g_{ij} \Big/ \sum_{k,l} W_{ijkl} f_{kl}^{(s)} \right)^{\lambda W_{ijkl} / \widetilde{W}_{kl}} \\
&\text{AART}: \quad f_{kl}^{(s+1)} = w_{kl} \cdot \left(f_{kl}^{(s)} + \lambda \frac{g_{ij} - \sum_{k,l} W_{ijkl} f_{kl}^{(s)}}{\|\mathbf{W}\|_F^2} \cdot \frac{\delta W_{ijkl}}{\widetilde{W}_{kl}} \right),
\end{aligned} \tag{15}$$

where $\widetilde{W}_{kl} = \sum_{i,j} W_{ijkl} \Big/ N_L$ is the reduced weight sum for the (k,l)-cell, N_L is the total number of strips used in reconstruction, and $\mathbf{w}$ is the matrix of correction factors which allow for a priori information on the object function (see below).

Step 2

$$f_{kl}^{(s+1)} = \frac{1}{(2r+1)^2} \sum_{m=-r}^{r} \sum_{n=-r}^{r} f_{k+m,l+n}^{(s+1)} \, \text{norm}(\widetilde{W}_{k+m,l+n}) \, \text{norm}(A_{k+m,l+n}), \tag{16}$$

where the integer r specifies the size $r \times r$ of the smoothing window, A_{kl} is the number of corrections to the solution element corresponding to the (k,l)-cell, and

$$\text{norm}(\xi_{kl}) = \left[\xi_{kl} - \min_{k,l}(\xi_{kl}) \right] \Big/ \left[\max_{k,l}(\xi_{kl}) - \min_{k,l}(\xi_{kl}) \right] \tag{17}$$

is the operator which normalizes the distributions $\{\widetilde{W}_{kl}\}$ and $\{A_{kl}\}$.

Accounting for the distributions of reduced weight sums and correction numbers over the cells is most crucial for DOT where they are markedly non-uniform (Figure 7). Figure 8 shows an example of reconstruction of the scattering object with two circular absorbing inhomogeneities 0.8 cm in diameters (see Section 3.2). Here and after the red triangles represent the localizations of the sources used for reconstruction. The Figure demonstrates advantages of the modified MART. We have bad results without taking into account the distributions $\{\widetilde{W}_{kl}\}$ and $\{A_{kl}\}$ (Figure 8 (b) and (c)).

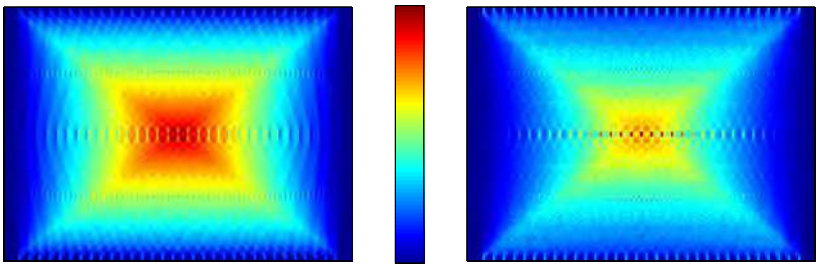

Figure 7. Distributions of reduced weight sums (a) and solution correction numbers (b) over 137×100 grid which cover the object shown in Figure 3

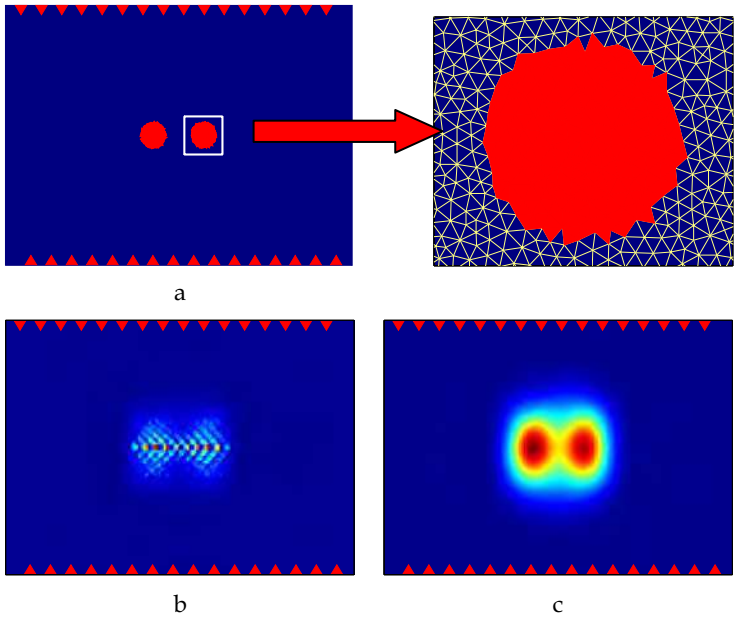

Figure 8. The 0.8-cm-in-diam absorbing inhomogeneities defined on a triangular mesh (a) and results of their reconstruction by the MART: without (b) and with (c) the distributions $\{\widetilde{W}_{kl}\}$ and $\{A_{kl}\}$

To use a priori information on the presence of structure-free zones in the reconstruction region, we developed an algorithm illustrated by Figure 9 which shows the reconstruction

of the middle section of the iron sphere compressed by an explosion from radiographic data (see Section 3.1). The algorithm is described by the following sequence of steps:

(a) Reconstruct the image $\{f_{kl}^1\}$ from projections corresponding to the first source only (Figure 9 (a)).

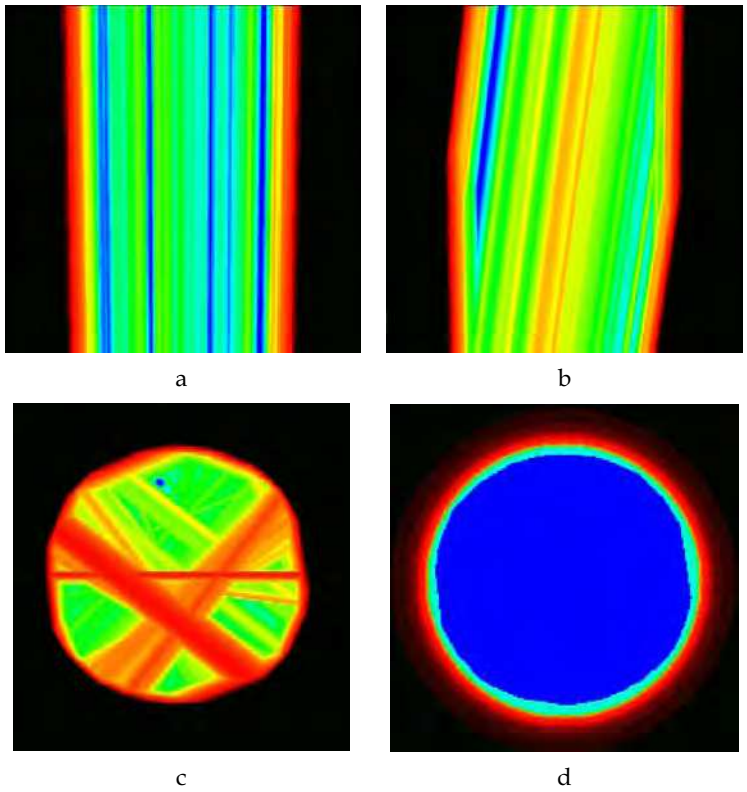

Figure 9. Generation of a useful part of the tomogram: (a) – the image $\{f_{kl}^1\}$; (b) – the image $\{\widetilde{f}_{kl}^2\}$; (c) – the image $\{\widetilde{f}_{kl}^{24}\}$; (d) – the set of multilevel regions

b) Reconstruct the image $\{f_{kl}^2\}$ from projections corresponding to the second source only and compare it with the result obtained at step (a). Following from the result of the comparison, form the image $\{\widetilde{f}_{kl}^2\}$ such that $\widetilde{f}_{kl}^2 = \min(f_{kl}^1, f_{kl}^2)$ for each (k,l)-cell (Figure 9(b)).

(c) Repeat step (b) for each following i-source forming the image $\{\widetilde{f}_{kl}^i\}$ such that $\widetilde{f}_{kl}^i = \min(\widetilde{f}_{kl}^{i-1}, f_{kl}^i)$ (Figure 9(c)). Search all given sources.

(d) For the last image $\{\widetilde{f}_{kl}^{last}\}$, define certain ascending sequence of relative thresholds $\{\varepsilon_m\}_1^M$, the largest of which does not exceed, for example, 0.1-0.2 and determine correction factors $\{w_{kl}\}$ using the following relations:

$$\begin{aligned} w_{kl} &= 0, \quad if \quad \widetilde{f}_{kl}^{last} < \varepsilon_1 \cdot \max\{\widetilde{f}_{kl}^{last}\}, \\ w_{kl} &= \frac{\varepsilon_m}{\varepsilon_M} \quad if \quad \varepsilon_m \cdot \max\{\widetilde{f}_{kl}^{last}\} \le \widetilde{f}_{kl}^{last} < \varepsilon_{m+1} \cdot \max\{\widetilde{f}_{kl}^{last}\} \\ w_{kl} &= 1, \quad if \quad \widetilde{f}_{kl}^{last} \ge \varepsilon_M \cdot \max\{\widetilde{f}_{kl}^{last}\}. \end{aligned} \tag{18}$$

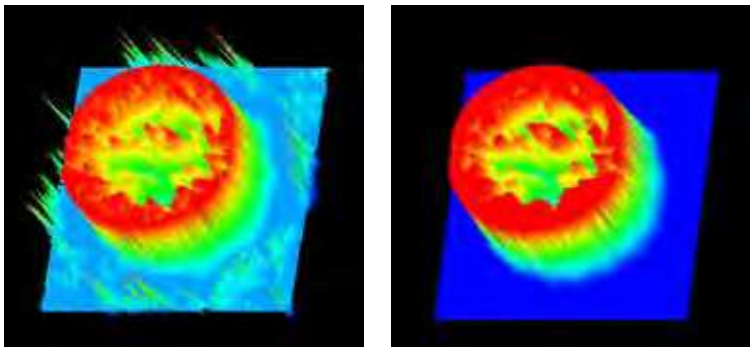

a b

Figure 10. Reconstructions of the sphere section from 24 views by the MART without (a) and with (b) the correction factors $\{w_{kl}\}$

Such a definition of the set of multilevel regions with values that monotonically decrease from unity to zero (Figure 9(d)) allows artifacts to be avoid in the structure-free zones, i.e. where the object function must be zero or close to zero. The effect of accounting for $\{w_{kl}\}$ is demonstrated in Figure 10 which illustrates the reconstruction of the section of a sphere from 24 views by the MART. For visual demonstration, reconstructions are presented as surface plots.

It should be noted that in the case of the AART, it is also appropriate to use a priori information on whether the reconstructed object function is non-negative. For this end, all negative elements in the solution approximation are changed by zeros at each iteration. In the case of the MART, this is not needed because the algorithm works with a priori positive values.

3. Examples of reconstruction of test objects and quantitative analysis of tomograms

3.1 Reconstruction of strongly absorbing structures from few X-ray views

This section gives examples of 2D reconstruction of objects with strongly absorbing structures from experimental radiographic data. The objects include

(a) a foam plastic cylinder 6 cm in diameter with periodical spatial structures in the form of rows of coaxial thin steel rods whose diameters are 1.5, 2.5, 5 and 8 mm, and
(b) an iron sphere 4.8 cm in diameter with lots of internal damages from shock compression.
X-ray projections are detected with a simple experimental setup (Figure 11 (a)). The radiation source is a pocket-size betatron with a small focal spot (about 1 mm) and a relatively small effective energy of the photon spectrum (about 2 MeV). The recording system combines a luminescent amplifying screen and an X-ray film. The object is placed between the source and the recording system so as to ensure that the film fully covers the object's shadow. To determine parameters of the characteristic curve of the recording system (photometric density versus exposure), we register the image of a step lead wedge with the object, as shown in Figure 11. Distances between the source and the object and between the source and the recording system are, respectively, 150 and 220 cm for the cylinder with periodic structures and 120 and 180 cm for the shocked sphere.

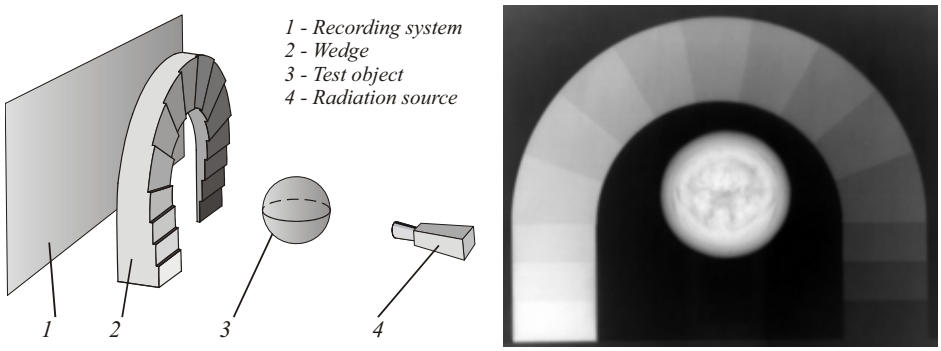

a b

Figure 11. Experimental setup (a) and X-ray photograph of the shocked iron sphere (b)

To collect information, each film with the X-ray image is scanned using a laser scanner with a small focal spot. Digital data collected are converted from scanner counts into film exposures with a technique (Kozlovskii, 2006) developed and experimentally adjusted at Russian Federal Nuclear Center – Zababakhin Institute of Applied Physics. The technique is based on the approximation of the characteristic curve by the relation

$$I = I_0 + I_{\max} \exp(-a \cdot |b - \lg H|^c), \tag{19}$$

where I is the photometric density, H is the exposure, I_0 is a parameter which characterizes the density of film fogging, $I_{\max}$ is a parameter which characterizes the maximum density the film permits, a and c are inclination and shape parameters, and b is a parameter which defines sensitivity of the recording system. The characteristic curve parameters I, $I_{\max}$, a, b and c are found through solving the problem of optimization for the objective function

$$\left[\frac{1}{Z} \sum_{i=1}^{Z} (I_i - I_i^{meas})^2 \right]^{1/2} \to \min, \tag{20}$$

where I_i is the photometric density calculated by expression (19) for i-step on the wedge, I_i^{meas} is the experimental density found with the image of the step wedge (Figure 11(b)) and Z is the number of steps on the wedge.

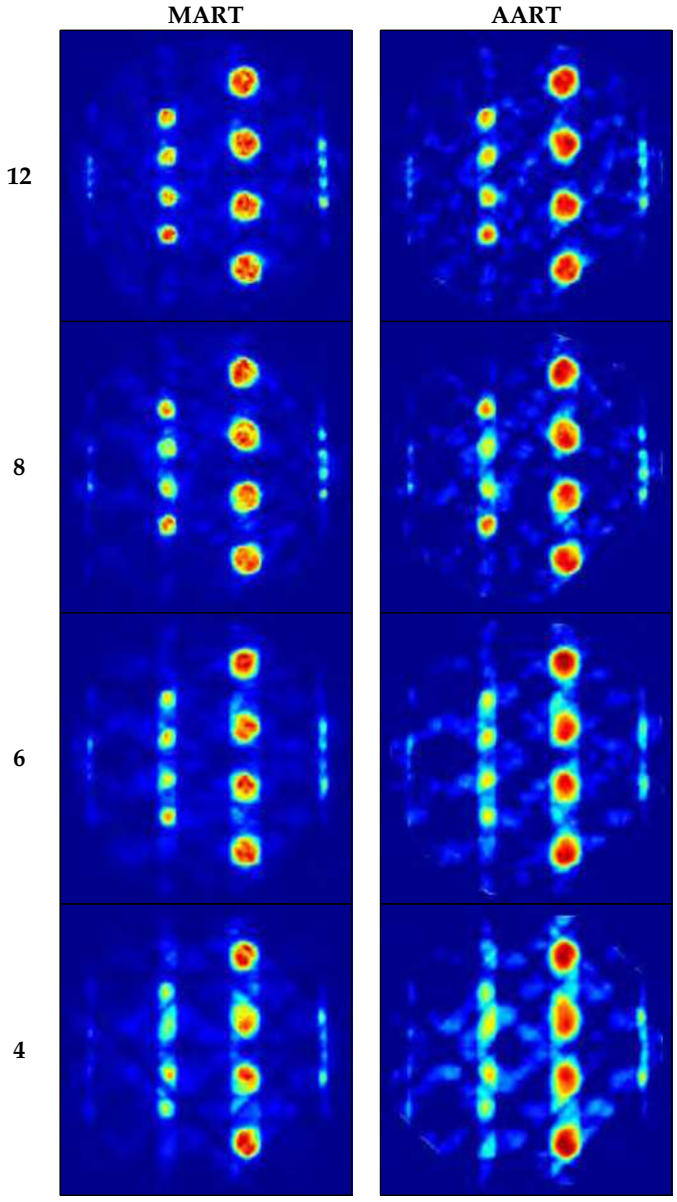

Figure 12. Tomograms of a cross section of the cylinder with periodic structures reconstructed from 12, 8, 6, and 4 views

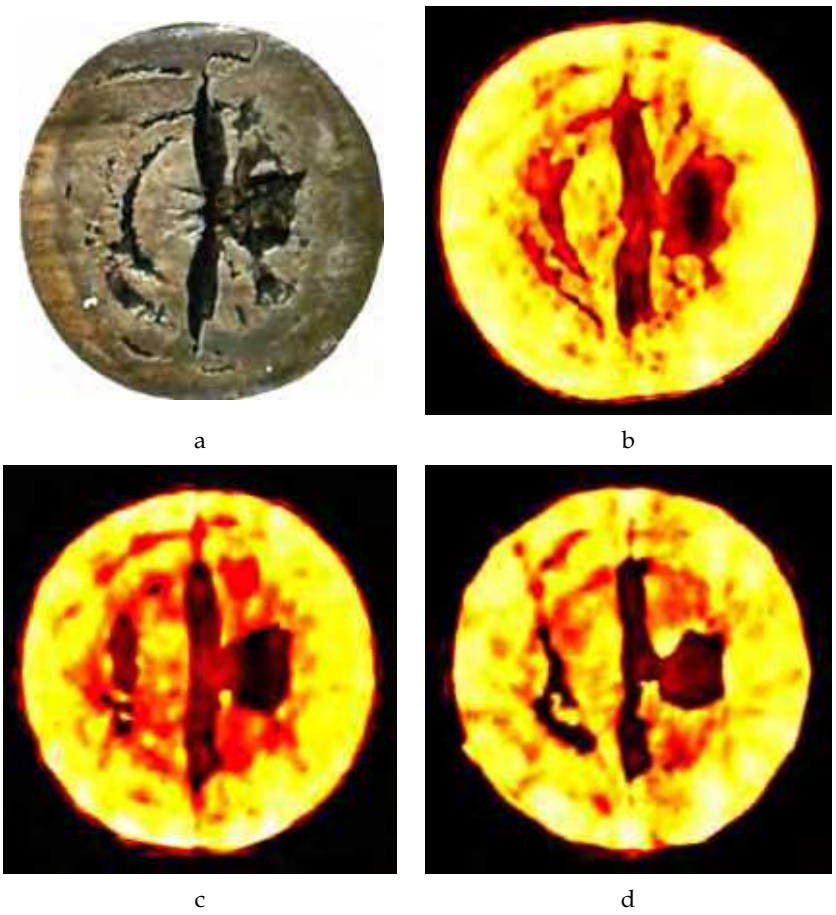

Figure 13. A photograph of the middle section of the sphere (a) and its reconstructions by the modified MART from 24 (b), 12 (c), and 8 (d) views

We assume that each X-ray in the conic beam is detected by a conventional receiver whose aperture is larger than the size of one cell of the digitized x-ray photograph. It is appropriate to take the aperture to be equal to the intrinsic resolution of the recording system. So, in order to calculate projections, we must average the exposures H over aperture areas. Projections are calculated as

$$g = -\log(H/H_0)\,, \tag{21}$$

where H_0 is film exposure without the object (background).

Figure 12 shows the tomograms of a cross section of the cylinder with periodic structures reconstructed from the 1D arrays of projections by the modified MART and AART described in Section 2.3. On the left of the Figure there are the numbers of views used for the reconstruction. It is seen that the quality of reconstructions by the entropy optimizing